Sound & Vibration 2025, 59(1), 1681.
https://doi.org/10.59400/sv1681

Article

Experimental and theoretical analysis of nonlinear acoustic characteristics of perforated acoustic liners

Yunpeng Liu[1,2], Peng Guo[1], Yibo Wang[1], Yingwen Yan[1,*]

[1] College of Energy and Power Engineering, Nanjing University of Aeronautics and Astronautics, Nanjing 210016, China
[2] Shenyang Aero Engine Research Institute, Aero Engine Corporation of China, Shenyang 110066, China
*** Corresponding author:** Yingwen Yan, yanyw@nuaa.edu.cn

CITATION

Liu Y, Guo P, Wang Y, Yan Y. Experimental and theoretical analysis of nonlinear acoustic characteristics of perforated acoustic liners. Sound & Vibration. 2025; 59(1): 1681. https://doi.org/10.59400/sv1681

ARTICLE INFO

Received: 3 September 2024
Accepted: 10 September 2024
Available online: 8 November 2024

COPYRIGHT

Copyright © 2024 by author(s). *Sound & Vibration* is published by Academic Publishing Pte Ltd. This work is licensed under the Creative Commons Attribution (CC BY) license. https://creativecommons.org/licenses/by/4.0/

Abstract: Perforated acoustic liner is one of the key components commonly used to suppress combustion oscillation in afterburners of military aircraft engines. The acoustic pressure generated by combustion oscillation is relatively high, and the nonlinear characteristics of these liners are significant. This paper employs both experimental and theoretical methods to study the nonlinear absorption coefficient and acoustic impedance of perforated acoustic liners in the range of 0 to 200 Pa. The results indicate that nonlinear effects increase the primary absorption frequency up to 70 Hz as the acoustic pressure amplitude rises from 2 Pa to 200 Pa. For small acoustic pressure amplitudes, it is recommended to use acoustic liners with smaller perforations, whereas for larger amplitudes, the perforation diameter should be increased ($d > 4$ mm). For liners with a perforation diameter of 1.1 mm, the inclination angle has little effect on the absorption coefficient. When the acoustic pressure amplitude is small, the acoustic liner has an optimal backing cavity height. However, at larger acoustic pressure amplitudes (200 Pa), increasing the backing cavity height is beneficial for the absorption coefficient. When the backing cavity height increased from 20 mm to 130mm, the absorption coefficient more than doubled. The nonlinear acoustic characteristics of perforated acoustic liners can provide valuable insights for the design of anti-vibration screens in afterburners.

Keywords: Perforated acoustic liner; passive suppression of combustion oscillation; nonlinear acoustics; absorption coefficient

1. Introduction

The afterburners of aircraft engines are prone to inducing combustion oscillation problems [1]. The anti-vibration screen in the afterburner, which is a typical perforated acoustic liner, can be used to suppress combustion oscillation that occurs within the flight envelope. Combustion oscillation can be suppressed from two perspectives: the dynamic characteristics of the flame and the acoustic characteristics. For the dynamic response of the flame, controlling the convective time is a crucial parameter for suppressing combustion oscillation [2–5]. Suppressing oscillations by controlling the flame requires complex methods to study the flame's response to acoustic excitation [6,7]. In comparison, the passive suppression of combustion oscillation using sound-absorbing structures is a commonly adopted method. These sound-absorbing structures primarily include Helmholtz resonators, perforated acoustic liners, quarter-wave tubes, and half-wave tubes.

Early research proposed that the principle of passive suppression involves reducing the growth rate of thermoacoustic instability in the system by introducing acoustic damping [8,9]. This can be simply understood as the sound-absorbing structure absorbing oscillatory pressure near the primary absorption frequency.

Acoustic theory suggests that when the acoustic impedance matches the traveling wave impedance of air, the sound-absorbing structure can fully absorb the sound waves. Therefore, the primary goal of most researchers is to optimize acoustic impedance to achieve a higher absorption coefficient or optimal acoustic damping [10]. The aperture size significantly impacts the acoustic resistance of the liners. To fine-tune the appropriate acoustic resistance, a perforated plate can be installed at the neck of a Helmholtz resonator [11]. Additionally, better damping characteristics can be achieved by altering the shape of the perforations [12] or by designing double-layer perforated plates [13,14]. Airflow can also adjust the acoustic impedance of the sound-absorbing structure. Jing [15] was the first to point out that an appropriate flow can increase acoustic resistance; however, an increase in the Mach number of the flow can lead to a deterioration in the damping performance of the sound-absorbing structure [16,17]. Under complex flow conditions or at high sound pressure amplitudes, it is necessary to recalibrate the effective length of the perforations, viscous wall dissipation, and vortex shedding coefficients [18]. Although various flow conditions affect the acoustic characteristics of the liners, Jakob et al. [19] pointed out that the acoustic resistance is more sensitive to the oscillatory velocity within the perforations.

Micro-perforated panels exhibit excellent sound absorption and noise reduction effects [20,21], but they may not perform as well under high sound pressure levels. In actual aircraft engine afterburners, the pressure pulsation amplitude of combustion oscillations is quite high, resulting in significant oscillatory velocities within the perforations and making the issue of nonlinear acoustic impedance particularly prominent. Perforations exhibit two distinct damping mechanisms: linear acoustic resistance and nonlinear acoustic resistance. When the pressure pulsation amplitude is relatively small, linear acoustic resistance predominates, primarily caused by boundary layer thermal losses and viscous losses. Flow instabilities can lead to vortex shedding at the shear layer near the perforations [22,23]. When the pressure pulsation amplitude is large, significant phenomena such as underdeveloped boundary layers and vortex shedding occur at the perforation edges, which are the main causes of nonlinear acoustic resistance [24]. Subsequent studies have found that features such as chamfered edges of perforations [25] and special structures in the neck [26] can significantly affect nonlinear acoustic resistance. It is important to note that the nonlinear effects of acoustic liners are generally concentrated near the primary absorption frequency, while the nonlinear components of acoustic impedance are relatively small when far from the absorption frequency [27].

Many researchers [28–30] have shown that perforated liner structures can effectively disrupt the coupling between sound waves and unsteady combustion heat release, significantly reducing the sound pressure amplitude in the combustion chamber, especially in the presence of crossflow. Gullaud [31], using a Helmholtz solver based on Howe's [32] model, solved the acoustic characteristics of perforated plates and calculated the acoustic modes in a combustion chamber with perforated plates. Meng [33] discovered that perforated plates with crossflow increase damping in swirl flame combustion instabilities, with two main mechanisms: sound attenuation and redistribution of the pressure modes and phases in the combustion chamber. The relative position of the absorber structures and the flame plays a critical role in

suppressing combustion instabilities [34]. Zalluhoglu [35] developed a unified thermoacoustic model of Helmholtz resonators arranged in various configurations to study the impact of their spatial distribution along a Rijke-type combustor on thermoacoustic instability. Betz et al. [36] examined the effects of the location and axial position of dampers in annular combustors on combustion instability, showing that dampers expand the stable combustion range. Dampers near the upstream flame are more effective, and asymmetric damper arrangements cause uneven acoustic mode attenuation. Altering the geometry of the annular combustor to disrupt symmetry significantly changes the limit cycle oscillation modes [37].

The anti-vibration screens in afterburners are structurally similar to Helmholtz resonators. The pressure pulsation amplitude generated by combustion oscillations is often quite large, making the issue of nonlinear acoustic impedance in acoustic liners particularly significant. Currently, there is little research on the effects of sound pressure amplitude on the nonlinear acoustic impedance of perforated acoustic liners. In previous related literature, nonlinear acoustic impedance theory studies similar to this paper have been mentioned. However, this paper focuses on the strong acoustic oscillations in the context of combustion oscillation, emphasizing the impact of sound pressure levels on the sound absorption characteristics of acoustic liners with different hole diameters, back cavities, and perforation inclination angles, which has been rarely addressed in past research. This research is of great importance for the design of perforated acoustic liners intended for use in environments with varying sound pressure levels.

2. Research subjects and experimental schedule

2.1. Research subject

Figure 1 shows a schematic diagram of the perforated acoustic liner, which consists of a perforated plate and a backing cavity. The thickness of the perforated plate L, the diameter d and number of perforations, and the dimensions of the backing cavity all influence the primary absorption frequency f and absorption coefficient α. The formula for calculating the primary absorption frequency f of the perforated acoustic liner is shown in Equation (1):

$$f = \frac{c_0}{2\pi}\sqrt{\frac{A}{Vl}} \tag{1}$$

where c_0 is the speed of sound, A is the total perforation area, V is the volume of the backing cavity, and l is the effective length of the perforation neck.

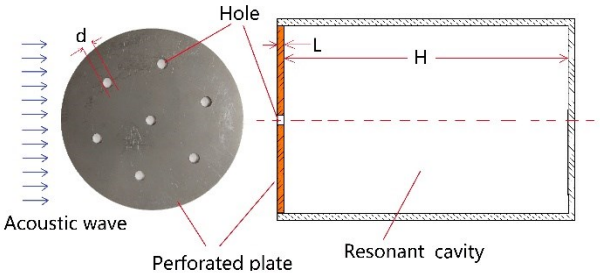

Figure 1. Schematic diagram of the perforated acoustic liner.

This study examines the effects of perforation diameter d, perforation inclination angle θ, and backing cavity height H on the acoustic absorption characteristics of the perforated plate resonator. The perforated plates are made of 304 stainless steels, and holes were created using laser processing on plates with a thickness of L = 1.8 mm. **Figure 2** shows the physical images of perforated acoustic liners with different structures used in the experiment. The perforated plates use an equilateral triangular perforation pattern, and **Figure 2n** provides a schematic diagram of the perforation inclination angle. There is a discrepancy between the actual hole sizes and the design dimensions. Detailed parameters are provided in **Table 1**. The perforated acoustic liners were manufactured using laser processing methods, and for cases with smaller diameters, the dimension errors are relatively larger.

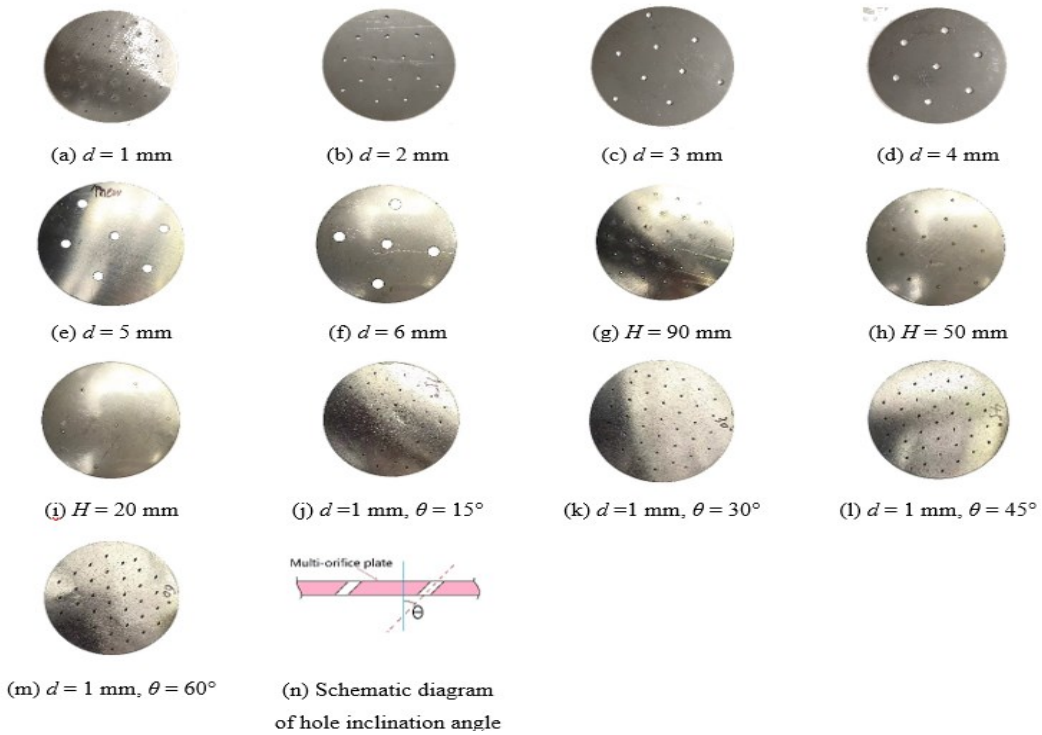

Figure 2. Physical images of the perforated acoustic liner.

Table 1. Geometric parameters of the perforated acoustic liner.

Case	Hole number	θ/degree	H/mm	d (designed)/mm	d (real)/mm	ε/%
1	39	0	130	1	1.08–1.20	0.980
2	15	0	130	2	2.11–2.19	1.400
3	9	0	130	3	3.17–3.20	1.890
4	7	0	130	4	4.19–4.21	2.564
5	6	0	130	5	5.18–5.20	3.356
6	5	0	130	6	6.16–6.20	3.965
7	27	0	90	1	1.06–1.08	0.679
8	15	0	50	1	1.06–1.08	0.378
9	6	0	20	1	1.07–1.08	0.150
10	39	15	130	1	1.06–1.09	0.980
11	39	30	130	1	1.08–1.12	0.980
12	39	45	130	1	1.07–1.11	0.980
13	39	60	130	1	1.08–1.12	0.980

2.2. Experimental schedule

The absorption coefficient of the perforated acoustic liner was measured using an impedance tube. The test system is shown in **Figure 3**, where the perforated acoustic liner is installed at the end of the impedance tube. The impedance tube is made of a very smooth inner-walled stainless steel pipe, with a total length of 700 mm and an inner diameter of 73 mm.

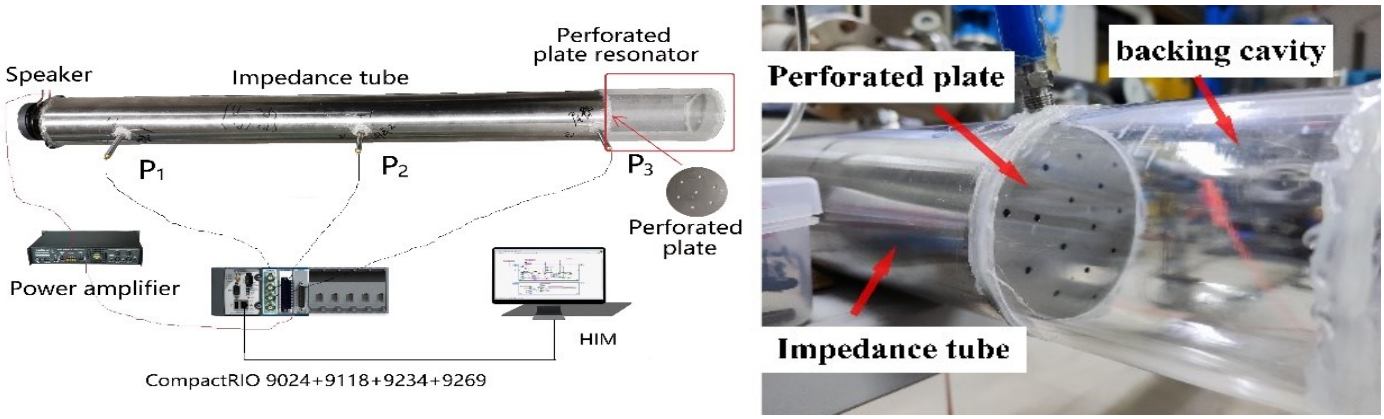

(a) Absorption coefficient experimental system **(b)** Perforated acoustic liner

Figure 3. Impedance tube experimental system.

A speaker is used as the sound source. Sound pressure transducers (MPA401 and MPA416) from Beijing Shengwang Company were used to measure acoustic pressure. The open-circuit sensitivity of the MPA416 transducer is 50 mV/Pa (± 2 dB), with a dynamic range of 29–127 dB, a background noise level below 29 dB. The maximum range is 44.8 Pa, the minimum acoustic pressure in this study is 2 Pa, and the maximum uncertainty is 0.0282%. The MPA401 transducer has an open-circuit sensitivity of 5 mV/Pa (± 2 dB), a dynamic range of 35–155 dB, a background noise level below 35 dB. The maximum range is 1124.7 Pa, the minimum measurable pressure is 40 Pa,

and the maximum uncertainty is 0.00281%. The sound pressure signals are synchronously sampled using an NI9234 data acquisition card from NI. The sampling frequency is 80 kHz, ensuring full-cycle sampling, with a single sampling time of 1 s, and 10 repeated measurements are averaged. The frequency range for the experimental study is 50–500 Hz, with a frequency interval of 10 Hz.

Three measurement points (P_1, P_2, P_3) are arranged in the impedance tube. Measurement point P_3 is located near the base of the acoustic liner. Due to the relatively small diameter of the standing wave tube, the sound wave can be simplified as a one-dimensional longitudinal wave, allowing the sound pressure at point P_3 to represent the sound pressure level of the acoustic liner. The acoustic pressure at measurement points P_1 and P_2 are measured, and the reflection coefficient at the end of the impedance tube are calculated using the two-microphone transfer function method [12]. The absorption coefficient is then:

$$\alpha = 1 - |r|^2 \tag{2}$$

By using the transfer function method to obtain the reflection coefficient *r*, the acoustic impedance can be determined as:

$$Zs = \frac{1+r}{1-r}\rho_0 c_0 \tag{3}$$

The comprehensive accuracy of the dynamic pressure sensors is less than 0.0282%. The uncertainty in the acoustic impedance *Zs*, calculated using error propagation, is 0.0798%, the uncertainty of absorption coefficient is 0.0127%.

3. Analysis of the absorption coefficient experimental results

3.1. Influence of perforation diameter

Figure 4 shows the absorption coefficients of the acoustic liner at different diameters and sound pressure amplitudes. The pressure marked in the figure represents the acoustic pressure of the acoustic liner. The acoustic resistance is influenced by both linear and nonlinear acoustic resistance due to air viscosity, with the latter being more pronounced at higher sound pressure levels. Linear acoustic resistance typically refers to the dissipation of sound energy due to viscous and thermal losses that remain constant regardless of the sound pressure level. Nonlinear acoustic resistance occurs when sound pressure levels are high enough that the resistance varies with amplitude, often due to phenomena like vortex shedding, flow separation, or other non-linear interactions within the acoustic liner. This distinction affects how the liner performs under different operating conditions and is essential for designing effective acoustic treatments that can handle varying sound pressure levels. Overall, nonlinear effects lead to an increase in the primary absorption frequency. As the acoustic pressure increases from 2 Pa to 200 Pa, the primary absorption frequency generally increases by 40 to 70 Hz, with the increase being more significant for acoustic liners with larger diameters. Considering the impact of the oscillation velocity within the holes mentioned bellow, the oscillation velocity amplitude is greater for acoustic liners with larger hole diameters, resulting in more pronounced shedding. This reduces the effective hole length, which may be a major reason for the increase in the primary

absorption frequency of the acoustic liner.

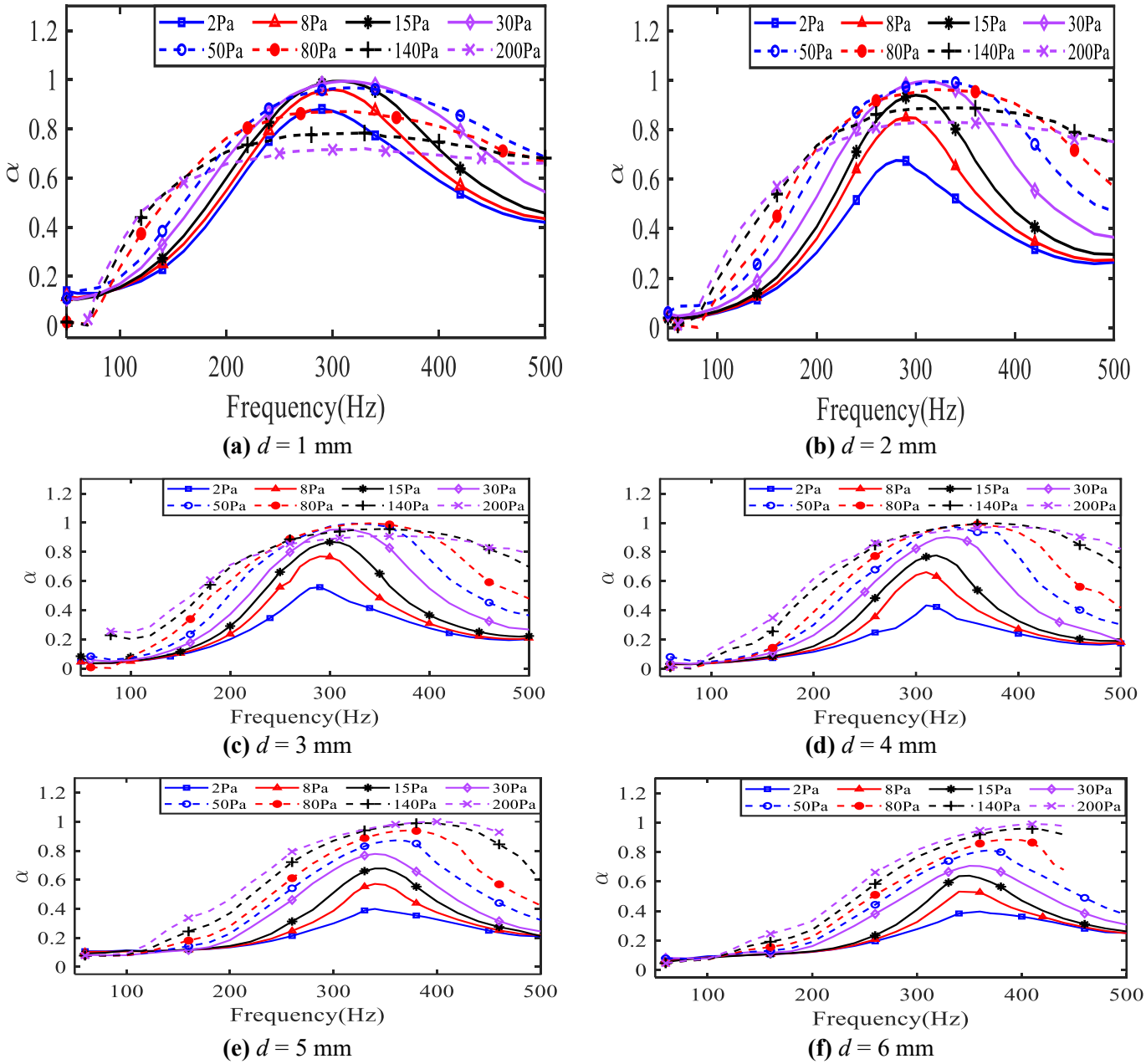

(a) $d = 1$ mm **(b)** $d = 2$ mm

(c) $d = 3$ mm **(d)** $d = 4$ mm

(e) $d = 5$ mm **(f)** $d = 6$ mm

Figure 4. Absorption coefficient of the acoustic liner under different acoustic amplitudes.

For smaller neck diameters ($d = 1$ mm and $d = 2$ mm), when the acoustic pressure exceeds 30 Pa, nonlinear acoustic resistance will weaken the absorption effects. When the acoustic pressure is higher, the acoustic liner exhibits a relatively wider absorption bandwidth. This effect is more pronounced for perforated plates with diameters greater than 1 mm. When the neck diameter of the perforated plate is relatively large, both linear and nonlinear acoustic resistances are small. Therefore, appropriately increasing the acoustic pressure can increase the nonlinear acoustic resistance of the perforated plate by increasing the oscillation velocity within the neck, bringing the impedance ratio at the outlet of the acoustic liner closer to the characteristic impedance of air.

The reflection coefficient is related to the acoustic impedance. It can be observed that there is an optimal acoustic impedance, which is the characteristic acoustic impedance of air ($\rho_0 c_0$), where the reflection coefficient is 0, and the absorption coefficient is 1, indicating that sound waves pass through the acoustic liner without reflection. However, if the acoustic impedance is too large or too small, reflections can occur, thereby reducing the absorption coefficient. Sound pressure levels mainly affect the nonlinear acoustic resistance of the acoustic liner, which gradually increases as the sound pressure level rises. Additionally, due to effects such as viscosity, the liner also exhibits linear acoustic resistance, especially when the orifice diameter is smaller, resulting in higher linear acoustic resistance. Therefore, when the orifice diameter is small (as in cases a–b), the linear acoustic resistance is significant and greater than the characteristic acoustic impedance of air. As the sound pressure level increases, the total acoustic impedance becomes larger, causing a continuous decrease in the absorption coefficient. In contrast, for liners with larger orifice diameters, the linear acoustic resistance is smaller. As the sound pressure level increases, the nonlinear acoustic resistance also increases, resulting in the absorption coefficient increasing with the sound pressure level or reaching an optimal sound pressure level.

To better understand the nonlinear acoustic impedance, the results of the oscillating velocity within the acoustic liner holes have been added, as shown in **Figure 5**. The absorption coefficient results in **Figure 4** indicate that with larger hole diameters, the influence of sound pressure level on nonlinear effects becomes more pronounced. When the hole diameter is small, the oscillating velocity inside the hole is not significant due to the impact of viscous effects. However, when the hole diameter is larger, the oscillating velocity inside the hole increases significantly with the increase in sound pressure level. Therefore, under different sound pressure levels, the oscillating velocity inside the hole is a key variable affecting the nonlinear sound absorption effects of the acoustic liner.

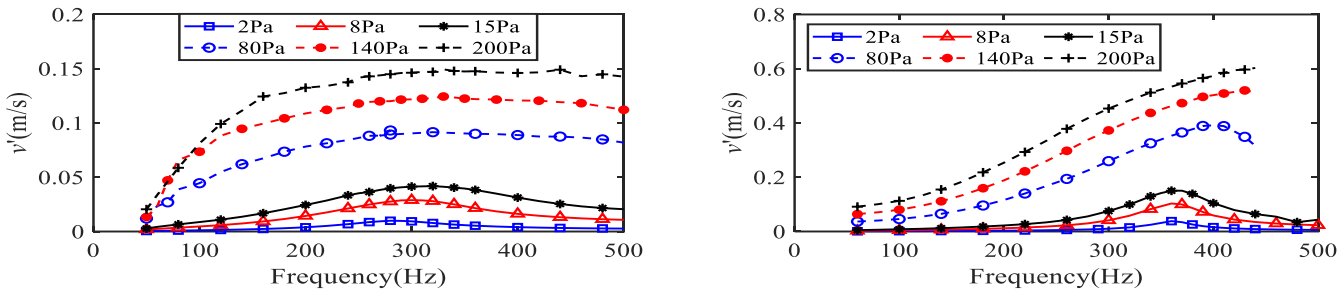

(a) d = 1 mm **(b)** d = 6 mm

Figure 5. Oscillating velocity amplitude within the liner holes.

Figure 6 presents the absorption coefficients under different perforation diameters. When the pressure amplitude is low, acoustic liners with smaller perforation diameters have higher absorption coefficients. This is because smaller perforation diameters result in higher linear acoustic resistance, and at lower sound pressure levels, the nonlinear acoustic resistance is minimal, bringing the total acoustic impedance of the liner closer to the optimal impedance ($\rho_0 c_0$). When the acoustic pressure is high, the nonlinear acoustic resistance increases, making it necessary to

reduce linear acoustic resistance to approach the optimal impedance. Therefore, acoustic liners with larger perforation diameters exhibit higher absorption coefficients. In summary, for different sound pressure levels, the absorption coefficient of the acoustic liner is influenced by both the perforation diameter and the sound pressure level. Smaller perforated plate resonators are recommended for low sound pressure levels, while larger perforation diameters should be used when the sound pressure level is high.

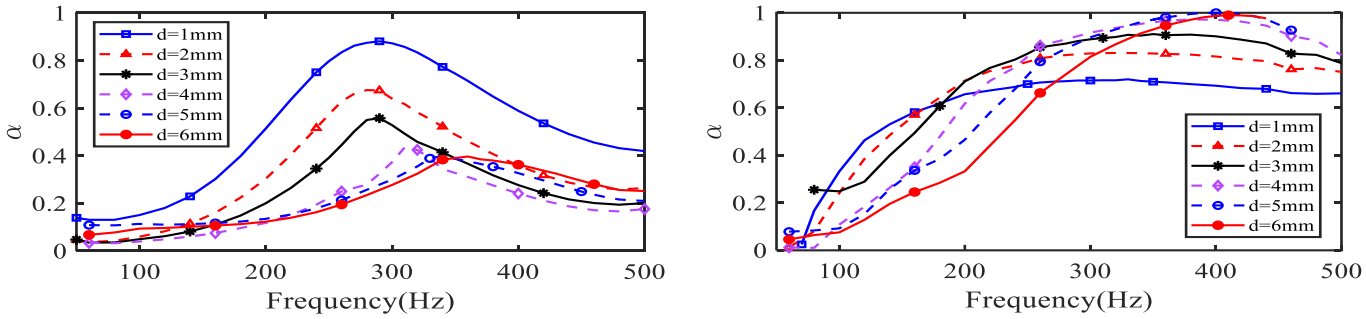

(a) P_3 = 2 Pa **(b)** P_3 = 20 Pa

Figure 6. Absorption coefficient of the acoustic liner under different perforation diameters.

Figure 7 shows the absorption coefficients at different sound pressure levels at 290 Hz. When the sound pressure amplitude is close to 0 Pa, the nonlinear effects can be neglected, resulting in a relatively low acoustic impedance ratio of the liner, and the liner does not achieve optimal absorption performance. Appropriately increasing the sound pressure amplitude can increase nonlinear acoustic resistance, and when the acoustic resistance approaches the optimal resistance, the maximum absorption coefficient is achieved.

Overall, perforated plates with smaller diameters can more quickly approach the optimal acoustic resistance and achieve the best absorption effect, but this effect diminishes rapidly afterward. On the other hand, perforated plates with larger diameters can maintain good absorption performance over a wider range of sound pressure levels. Therefore, in environments with high sound pressure levels, it is beneficial to choose acoustic liners with larger perforation diameters.

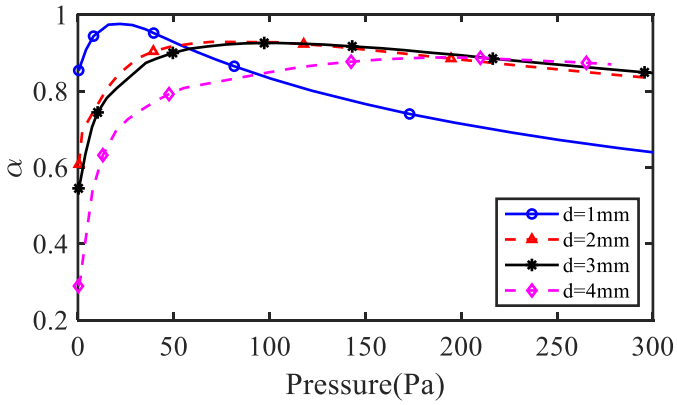

Figure 7. The variation pattern of the absorption coefficient with acoustic amplitude.

3.2. The influence of perforation angle

In the high-temperature components of aircraft engines, cooling is often a critical consideration. Multi-angle perforations offer relatively high cooling efficiency and are commonly used in the main combustion chamber and afterburner of gas turbines. This study takes a perforated plate with a diameter of d = 1 mm as an example. **Figure 8** shows the influence of the perforation inclination angle on the absorption coefficient of the perforated plate resonator. The results indicate that for acoustic liners with d = 1 mm, the perforation inclination angle has a minimal impact on the absorption coefficient. The inclination angle of the perforations changes the direction of the incident sound waves, thereby affecting the path of the sound waves entering the perforated structure. The correction of the perforation length is one of the key factors influencing the results. Although the inclination angle changes the geometric length of the perforations in the acoustic liner, the presence of acoustic radiation on both sides of the liner necessitates a correction of the actual perforation length, which becomes more complex with the inclination. The mechanism by which the inclination angle of the perforations affects the sound absorption coefficient of the acoustic liner is a complex process involving multiple factors. It requires systematic analysis and research considering the specific material properties, sound wave frequency, incident angle, and geometric parameters of the perforation structure.

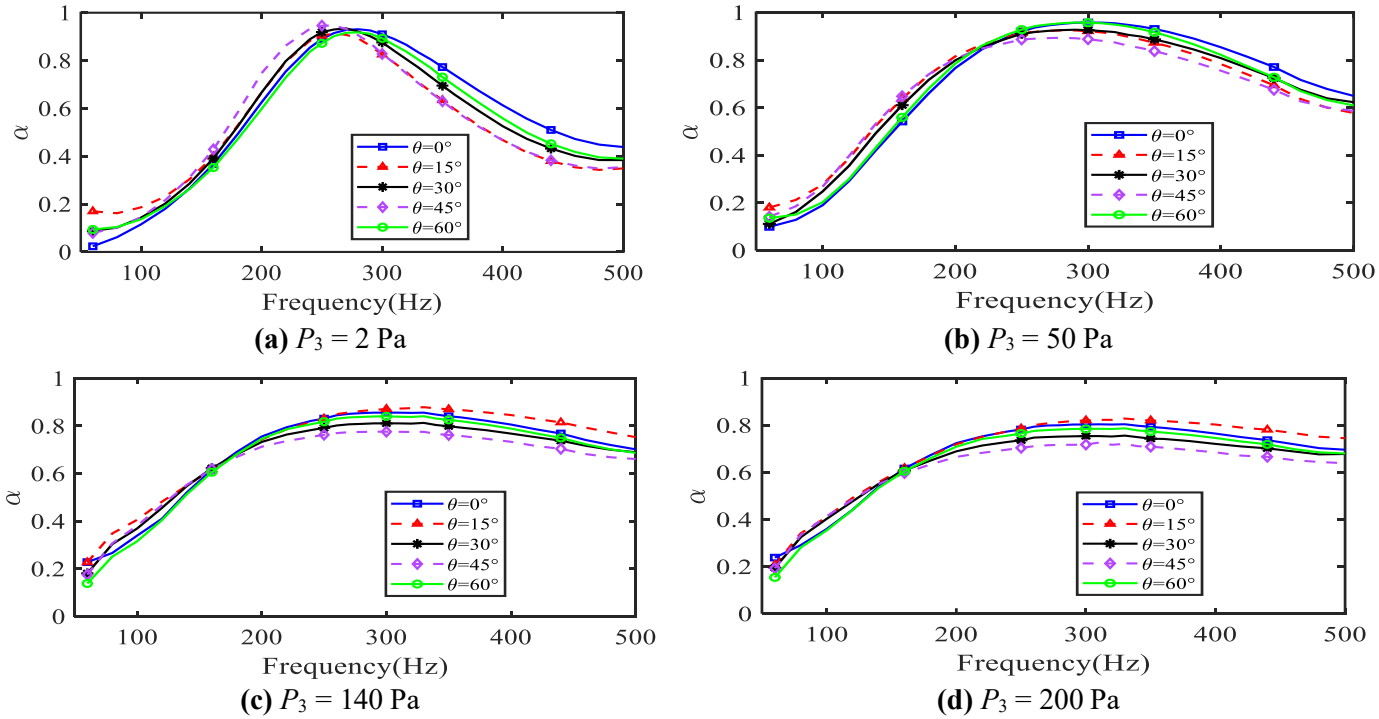

(a) P_3 = 2 Pa **(b)** P_3 = 50 Pa

(c) P_3 = 140 Pa **(d)** P_3 = 200 Pa

Figure 8. Absorption coefficient of perforated plates with different inclination angles (d = 1 mm).

3.3. The influence of backing cavity height

In engineering applications, the dimensions of the backing cavity are often constrained. Although the desired primary absorption frequency can be achieved by adjusting parameters such as perforation diameter and perforation rate, the absorption coefficient can vary significantly. When the perforated plate diameter d = 1 mm, the

absorption coefficients under different backing cavity heights are shown in **Figure 9**. When the perforation diameter of the acoustic liner is fixed, the number of perforations (perforation rate) should be adjusted to achieve the same primary absorption frequency.

The experimental results indicate that when the sound pressure amplitude is low, there is an optimal backing cavity height for the acoustic liner. Both smaller and larger backing cavity heights reduce the absorption coefficient. However, when the sound pressure amplitude is high, increasing the backing cavity height is beneficial for the absorption coefficient. At an acoustic pressure P_3 = 200 Pa, increasing the backing cavity height from 20 mm to 130 mm more than doubles the absorption coefficient. When the acoustic pressure is relatively low, moderately reducing the backing cavity height may be advantageous, but a backing cavity height that is too small is not recommended, as it results in low absorption coefficients under different sound pressure levels.

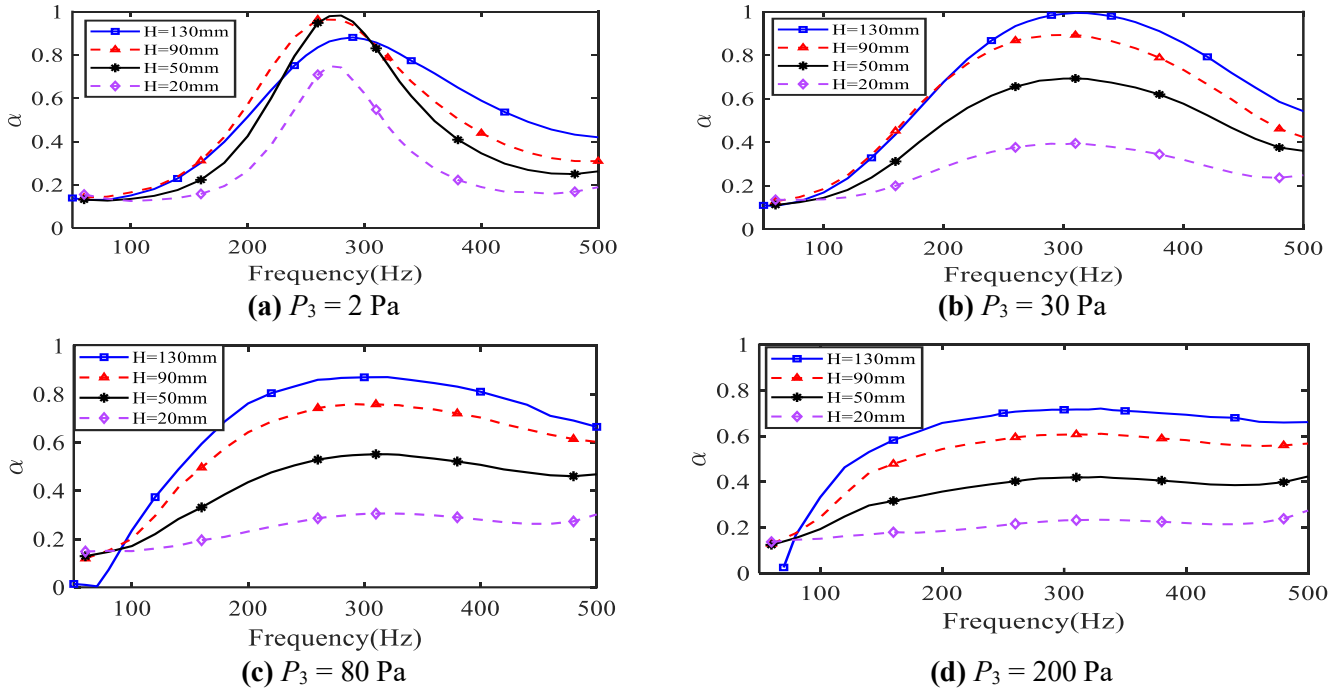

(a) P_3 = 2 Pa **(b)** P_3 = 30 Pa

(c) P_3 = 80 Pa **(d)** P_3 = 200 Pa

Figure 9. The effects of backing cavity height on the absorption coefficient (d = 1 mm).

4. Theoretical analysis of the nonlinear characteristics of perforated acoustic liners

A perforated acoustic liner can be simplified as multiple Helmholtz resonators connected in parallel. A Helmholtz resonator consists of a neck and a backing cavity. The acoustic impedance at the outlet of the Helmholtz resonator can be calculated using the impedance transfer formula:

$$Zs_0 = \rho_0 c_0 \frac{Zs_l + j\rho_0 c_0 \tan(kl)}{\rho_0 c_0 + jZs_l \tan(kl)} \tag{4}$$

where Zs_l is the terminal acoustic impedance, ρ_0 is the air density, c_0 is the speed of sound, k is the wave number, and l is the length. When viscosity is not considered and assuming the end of the backing cavity is a rigid wall with an acoustic impedance Zs_l of infinity, the acoustic impedance at the neck's end near the backing cavity can be

first obtained using Equation (4). Then, by substituting this result back into Equation (4), the acoustic impedance at the outlet of the acoustic liner can be calculated. Due to the effect of sound radiation, the depth of the perforation needs to be corrected, with the effective depth given by $l_{real} = l + \lambda d$, where d is the diameter of the perforation, l is the geometric depth of the perforation, and the coefficient is $\lambda = 8/(3\pi)$ [38,39]. With the speed of sound c_0 = 340 m/s and density ρ_0 = 1.2 kg/m^3, these calculations apply to the perforated acoustic liners with the parameters of Case 9 listed in **Table 1**.

When the perforation diameter is small, the air viscosity effect inside the perforation is significant, which will increase the acoustic resistance of the small tube and alter the acoustic impedance at the tube's opening as well as the primary absorption frequency. When the velocity oscillation inside the cylindrical tube is large, the one-dimensional momentum equation within the cylindrical duct is as follows [40]:

$$-\frac{\partial p'}{\partial z} = (R + \eta_0|V|)v' + M \cdot i\omega v' \tag{5}$$

where p' represents the pressure oscillation, v' represents the velocity oscillation, R is the acoustic resistance, M is the acoustic mass, $|V|$ is the root mean square of the particle oscillation velocity, ω is the angular frequency, and η_0 is the static nonlinear coefficient. The term $\eta_0|V|$ in Equation (5) is the nonlinear term, and the part of the equation on the right-hand side, excluding the nonlinear term, is solved using Equation (6):

$$\rho_0 \frac{\partial v}{\partial t} = -\nabla p + \mu \Delta v \tag{6}$$

Finally, we obtain:

$$\frac{\partial p'}{\partial z} = i\omega\rho_0 \left[1 - \frac{2}{s\sqrt{-i}} \frac{J_1 s\sqrt{-i}}{J_0 s\sqrt{-i}}\right]^{-1} v' + \eta 0 \bar{v} v' \tag{7}$$

where $s = d/\sqrt{2}\delta$, δ represents the thickness of the viscous boundary layer, $\delta = 2\mu/(\omega\rho_0)$, J_0 and J_1 denote the 0th and 1st order Bessel functions, $\bar{v}$ represents the mean flow velocity or the root mean square of the oscillation velocity. When the perforation depth is small, Equation (7) can be simplified to:

$$p_1^{'} - p_2^{'} = l_{real} v'(G + \eta_0 \bar{v}) \tag{8}$$

where $G = i\omega\rho_0\left[1 - (2/s\sqrt{-i})(J_1(s\sqrt{-i})/J_0(s\sqrt{-i}))\right]^{-1}$, At the interface between the acoustic liner and the backing cavity, the continuity equation is satisfied as follows:

$$\rho_1 S_1 v_1^{'} = \rho_2 S_2 v_2^{'} \tag{9}$$

where $v_1^{'}$ and $v_2^{'}$ represent the velocity oscillations on the left and right sides of the resonator interface, respectively. Additionally, the pressure on both sides of the cross-section at the interface between the acoustic liner and the backing cavity is equal, i.e., $p_1^{'} = p_2^{'}$. The above equations describe the relationship between $v_1^{'}$ and $v_2^{'}$. Combined with Equation (4), the acoustic impedance at the resonator interface satisfies:

$$\frac{p_2^{'}}{v_2^{'}} = \frac{p_1^{'} S_2}{v_1^{'} S_1} = -i\rho_0 c\, cot(kH) \tag{10}$$

Combining Equations (8) and (10), the acoustic impedance Zs at the resonator outlet is obtained as:

$$Zs = \frac{p_0^{'}}{S_1 v_1^{'}} = \frac{l_{real}}{S_1}(G + \eta_0 \bar{v}) - i\rho_0 c \cdot \frac{1}{S_2} cot(kH) \tag{11}$$

where S_1 represents the cross-sectional area of the neck, and S_2 represents the cross-sectional area of the cavity.

Additionally, from observing Equation (7), $-\partial p'/(\partial z v')$ represents the static flow resistivity of the material, which is the pressure drop per unit length and unit velocity as air flows through the material. For small disturbances, the linear static flow resistivity is $\sigma = 32\ \mu/d^2$, where μ is the air viscosity coefficient, with $\mu = 1.8 \times 10^{-5}$ Pa/s under standard conditions. Equation (11) expresses the nonlinear momentum equation, where $\eta_0 \bar{v}$ is the nonlinear term. The nonlinear component can be obtained by subtracting the linear static flow resistivity from the total static flow resistivity measured in experiments. Thus, $l_{real}\eta_0 \bar{v}/S_1$ represents the nonlinear acoustic impedance.

Before calculating the acoustic impedance at the outlet of the Helmholtz resonator, it is essential to first measure the static flow resistivity of the neck, especially when the neck diameter is small, as the static flow resistivity becomes significant. At higher sound pressure levels, the nonlinear acoustic resistance will be substantial. For the case with a neck length of l = 1.8 mm and a neck diameter of d = 1.1 mm, it is challenging to measure the static flow resistivity of a single small hole accurately. Therefore, the static flow resistivity of a perforated plate with a certain perforation rate (ε = 0.980%) is measured. The airflow is measured using a standard orifice flowmeter with an accuracy of 1.02%, and the average velocity through the small holes is calculated. The pressure difference across the perforated plate is measured using a differential pressure transmitter with an accuracy of 0.5%, and the resulting nonlinear coefficient η_0 is shown in **Figure 10**.

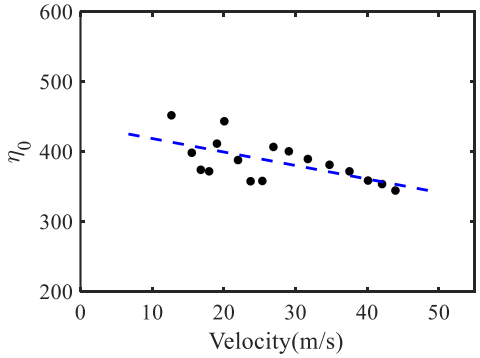

Figure 10. Nonlinear coefficient of the perforated acoustic liner (d = 1.1 mm).

Based on the flow resistance characteristics of the acoustic liner, the definition of the acoustic impedance ratio $Zs = p'/v'$, and Equation (10), the acoustic pressure amplitude at the resonator's mouth is set to 20 Pa. Through iterative calculations, the

acoustic impedance at the outlet of the acoustic liner is obtained, as shown in **Figure 11**. The results indicate that the acoustic impedance increases when viscosity is considered, especially near the resonance frequency, while the change in acoustic impedance ratio is more gradual when deviating from the resonance frequency.

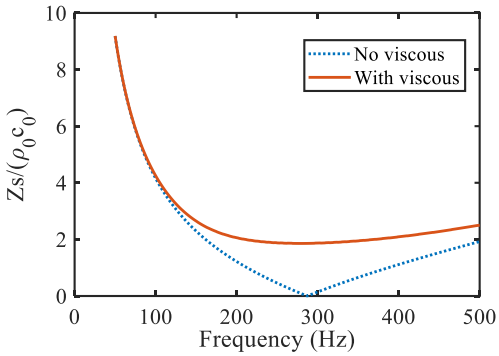

Figure 11. Acoustic impedance ratio at the outlet of the Helmholtz resonator.

Figure 12 presents the acoustic impedance of the acoustic liner with a diameter of 1.1 mm, as derived theoretically and measured experimentally. The geometric parameters are detailed in **Table 1** (serial number 1). The results show good agreement at lower sound pressure levels, indicating that the calculation of the acoustic impedance is fairly accurate. However, there is some deviation at higher sound pressure levels. Firstly, simplifying the acoustic liner as multiple independent Helmholtz resonators is not sufficiently accurate, as there is mutual interference between the holes of the actual acoustic liner. Additionally, there are deviations in the correction of the orifice length under high sound pressure level conditions, where nonlinear effects are significant. Overestimating the correction coefficient for orifice length will increase the theoretical value of the acoustic impedance. Furthermore, when measuring the flow resistance coefficient of the acoustic liner, the airflow velocity inside the holes is inferred from the airflow rate. At low flow velocities, the measurement error of the airflow rate is relatively large, which leads to an overestimation of the nonlinear coefficient. Consequently, the theoretical value of the acoustic impedance is overestimated. Additionally, within a highly oscillatory velocity field, periodic oscillating jets occur inside the perforated plate, and vortex separation effects can alter the acoustic impedance characteristics of the perforated plate. Overall, the theoretically derived acoustic impedance ratio of the acoustic liner matches well with the experimental results, confirming the accuracy of the theoretical analysis.

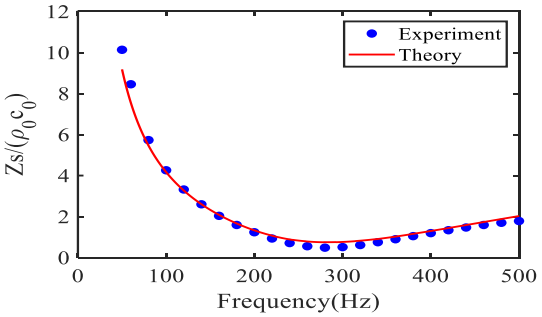

(a) P_3 = 2 Pa

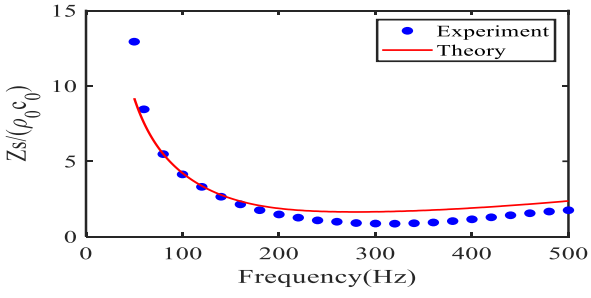

(b) P_3 = 30 Pa

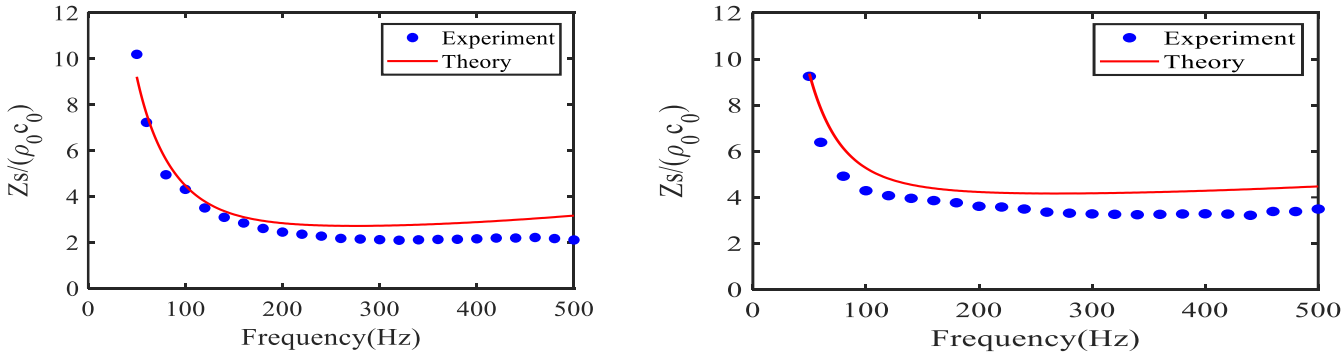

(c) P_3 = 80 Pa **(d)** P_3 = 200 Pa

Figure 12. Acoustic impedance ratio of the perforated plate resonator (d = 1.1 mm).

A perforated acoustic liner is equivalent to multiple Helmholtz resonators connected in parallel. The more Helmholtz resonators that are paralleled, the lower the acoustic impedance of the liner. However, a lower acoustic impedance is not always better; the optimal condition is when the acoustic impedance ratio satisfies $Zs = \rho_0 c_0$, at which point no reflection occurs at the perforated plate, resulting in the maximum sound absorption coefficient. **Figure 13** shows the acoustic impedance at the outlet of the perforated plate for different backing cavity heights. When the sound pressure level is low, increasing the backing cavity height is equivalent to connecting more Helmholtz resonator units in parallel, thereby gradually reducing the acoustic impedance ratio until it approaches $\rho_0 c_0$ at H = 90 mm, achieving the optimal sound absorption coefficient.

However, under high acoustic pressure conditions, the nonlinear effects of the oscillating air within the perforations significantly increase the acoustic impedance ratio of the liner. Even with further increases in backing cavity height, it is difficult to achieve the optimal acoustic impedance ratio ($Zs = \rho_0 c_0$). Ideally, continuing to increase the backing cavity height would further improve the absorption coefficient, but this is often impractical in engineering applications. These results indicate that extremely small backing cavity heights are not recommended. This is because they correspond to a smaller number of effective Helmholtz resonator units (lower perforation ratio). This results in an acoustic impedance that is significantly higher than the optimal impedance, leading to poor acoustic absorption performance.

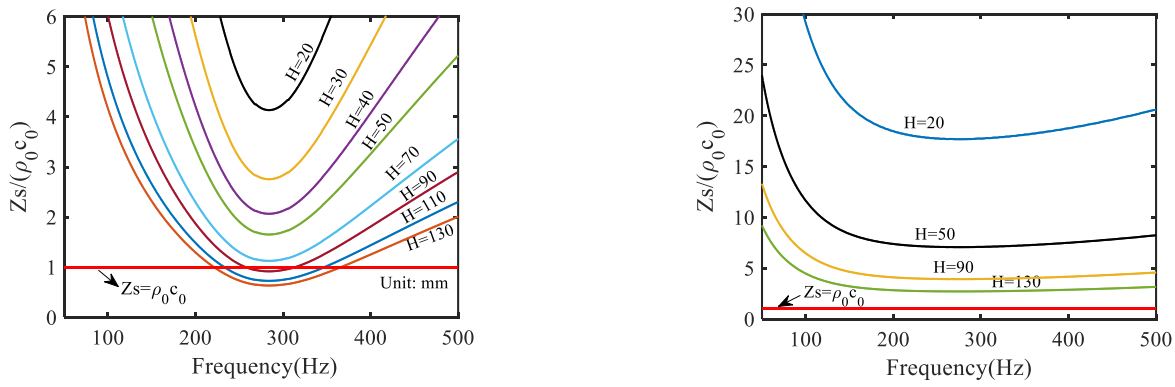

(a) P_3 = 2 Pa **(b)** P_3 = 80 Pa

Figure 13. Acoustic impedance at the outlet of the acoustic liner (theoretical, d = 1 mm).

Previous experimental results indicate that different sound pressure levels significantly impact the optimal performance of perforated plates, which is attributed to the effect of sound pressure on the nonlinear acoustic resistance of the perforated plates. **Figure 14** illustrates the acoustic impedance of the liner under different sound pressure levels at point P_3. The results indicate that as the sound pressure level increases, the acoustic impedance gradually increases, due to the increasing nonlinear acoustic resistance. As the acoustic impedance approaches $\rho_0 c_0$, there is no reflection of the sound waves, leading to the optimal sound absorption coefficient. However, further increases in sound pressure levels will reduce the sound absorption coefficient. Therefore, the perforated plate resonator has an optimal environmental sound pressure level for application.

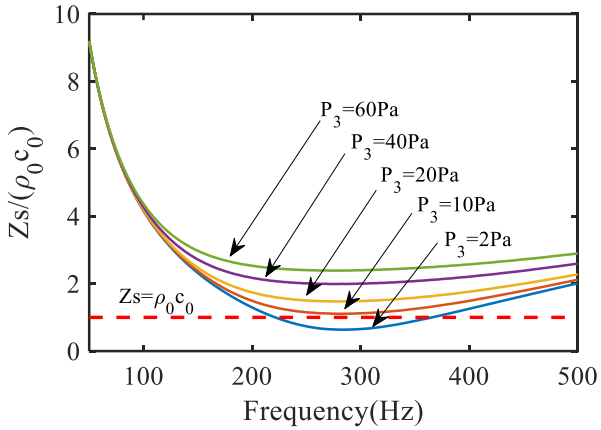

Figure 14. Acoustic impedance under different sound pressure levels (H = 130 mm, d = 1 mm).

5. Discussion

This study investigated the influence of sound pressure levels, aperture diameter, perforation angle, and backing cavity height on the sound absorption coefficient of perforated acoustic liners, and analyzed the mechanism of how changes in acoustic impedance affect the sound absorption coefficient through theoretical analysis. The main findings are as follows:

1) As the sound pressure level increases, the nonlinear acoustic resistance of the perforated acoustic liner significantly increases. The impact of this increase on the sound absorption coefficient varies with different aperture sizes. The dominant oscillation frequency generally increases by 40–70Hz as the sound pressure level increases.

2) The aperture size significantly affects the sound absorption coefficient under different sound pressure levels. When the sound pressure level is low, a perforated resonator with smaller apertures is recommended, while larger apertures are preferable at higher sound pressure levels.

3) For perforated acoustic liners with an aperture diameter of 1.1 mm, the perforation angle has a relatively minor effect on the sound absorption coefficient.

4) When the sound pressure level is relatively low, moderately reducing the backing cavity height can potentially increase the sound absorption coefficient.

Conversely, increasing the backing cavity height is beneficial for enhancing the sound absorption coefficient at higher sound pressure levels.

5) Nonlinear acoustic resistance is the key mechanism, through which sound pressure levels and geometrical parameters can significantly affect the sound absorption coefficient of the acoustic liner.

Author contributions: Conceptualization, YL and YY; methodology, YL and PG; investigation, YL and PG; writing, YL and YW. All authors have read and agreed to the published version of the manuscript.

Funding: This work received funding from 1) the National Major Science and Technology Projects of China (J2022-III-0007), 2) Industry-Academia-Research Collaboration Project "Study on the Construction of a Combustion Oscillation Calculation Model and Suppression Technology for Afterburners" funded by the China Aero Engine Corporation (Project Number HFZL2022CXY009) and 3) China "Huiyan Action" Innovation Achievement Transformation and Application Project "Active and Passive Suppression Methods for Combustion Oscillation in Aircraft Engine Afterburners".

Conflict of interest: The authors declare no conflict of interest.

Nomenclature

A	Total perforation area
c_0	Speed of sound
d	Perforation diameter
f	Primary absorption frequency
H	Backing cavity height
k	Wave number of acoustic wave
L	Thickness of the perforated plate
l	Length of the perforation neck
l_{real}	Effective length of the perforation neck
M	Acoustic mass
P_3	Acoustic pressure amplitude at the perforated plate end
p'	Pressure oscillation
R	Acoustic resistance
r	Acoustic reflection coefficient
s	Distance between point P_1 and point P_2
V	Volume of the backing cavity
$\|V\|$	Mean square of the particle oscillation velocity
$\bar{v}$	Mean flow velocity
v'	Velocity oscillation
x_1	Distance from the sample to P_1
x_2	Distance from the sample to P_2
Zs	Acoustic impedance of acoustic liner
α	Absorption coefficient

ε	Perforation ratio
ρ_0	Air density
θ	Perforation inclination angle
ω	Angular frequency
δ	Thickness of the viscous boundary layer
μ	Air viscosity coefficient
η_0	Nonlinear coefficient

References

1. Smith G, Henderson R. Combustion instability in a turbofan mixed-flow augmentor. In: Proceedings of 8th Joint Propulsion Specialist Conference; 1972; New Orleans, LA, USA.
2. Yu Z, Xu Y. Analysis of Thermoacoustic Instabilities Using the Helmholtz Method in a Swirled Premixed Combustor. Processes. 2024; 12(4): 741. doi: 10.3390/pr12040741
3. Cheng J, Liu B, Zhu T. Characterizing combustion instability in non-premixed methane combustion using internal flue gas recirculation. Applied Energy. 2024; 370: 123602. doi: 10.1016/j.apenergy.2024.123602
4. Wei D, Fang H, Zhou H. Investigation on self-excited thermoacoustic instability and emission characteristics of premixed CH4/NH3/air flame. Thermal Science and Engineering Progress. 2024; 51: 102614. doi: 10.1016/j.tsep.2024.102614
5. Kim S, Kim D. Analytical modeling of thermoacoustic instability influences in gas turbine combustors: A detailed parameter sensitivity analysis. Case Studies in Thermal Engineering. 2024; 59: 104595. doi: 10.1016/j.csite.2024.104595
6. Shi X, Zhang J, Zhang Y, et al. Combustion and extinction characteristics of an ethanol pool fire perturbed by low–frequency acoustic waves. Case Studies in Thermal Engineering. 2024; 60: 104829. doi: 10.1016/j.csite.2024.104829
7. Yu M, Jiang G, Jiang Y, et al. Experimental and numerical study of convective heat transfer in-line tube bundle by acoustic action. Case Studies in Thermal Engineering. 2023; 44: 102869. doi: 10.1016/j.csite.2023.102869
8. Noiray N, Schuermans B. Theoretical and experimental investigations on damper performance for suppression of thermoacoustic oscillations. Journal of Sound and Vibration. 2012; 331(12): 2753-2763. doi: 10.1016/j.jsv.2012.02.005
9. Kelsall G, Troger C. Prediction and control of combustion instabilities in industrial gas turbines. Applied Thermal Engineering. 2004; 24(11-12): 1571-1582. doi: 10.1016/j.applthermaleng.2003.10.025
10. Bourquard C, Noiray N. Stabilization of acoustic modes using Helmholtz and Quarter-Wave resonators tuned at exceptional points. Journal of Sound and Vibration. 2019; 445: 288-307. doi: 10.1016/j.jsv.2018.12.011
11. Pandalai R, Mongia H. Combustion instability characteristics of industrial engine dry low emission combustion systems. In: Proceedings of 34th AIAA/ASME/SAE/ASEE Joint Propulsion Conference and Exhibit; 13–15 July 1998; Cleveland, OH, USA.
12. Zhao D, Ji C, Wang B. Geometric shapes effect of in-duct perforated orifices on aeroacoustics damping performances at low Helmholtz and Strouhal number. The Journal of the Acoustical Society of America. 2019; 145(4): 2126-2137. doi: 10.1121/1.5096642
13. Kim D, Jung S, Park H. Acoustic damping characterization of a double-perforated liner in an aero-engine combustor. Journal of Mechanical Science and Technology. 2019; 33(6): 2957-2965. doi: 10.1007/s12206-019-0544-2
14. Zhou H, Meng S, Tao C, et al. Low-frequency sound absorptive properties of dual perforated plates under bias flow. Applied Acoustics. 2019; 146: 420-428. doi: 10.1016/j.apacoust.2018.11.027
15. Jing X, Sun X. Effect of Plate Thickness on Impedance of Perforated Plates with Bias Flow. AIAA Journal. 2000; 38(9): 1573-1578. doi: 10.2514/2.1139
16. Wu G, Lu Z, Xu X, et al. Numerical investigation of aeroacoustics damping performance of a Helmholtz resonator: Effects of geometry, grazing and bias flow. Aerospace Science and Technology. 2019; 86: 191-203. doi: 10.1016/j.ast.2019.01.007
17. Wu G, Guan YH, Ji C, et al. Experimental studies on sound absorption coefficients of perforated pipes with bias-grazing flows at low Mach and Strouhal number. Aerospace Science and Technology. 2020; 107: 106255. doi: 10.1016/j.ast.2020.106255
18. Yu Z, Yang Y. Investigation of thermoacoustic oscillation attenuation by modified Helmholtz dampers with dual frequency bands. Applied Acoustics. 2022; 185: 108433. doi: 10.1016/j.apacoust.2021.108433

19. von Saldern JGR, Eck MEG, Beuth JP, et al. Acoustic characteristics of impingement cooling sheets; effect of bias-grazing flow interaction on the liner impedance in a thin annulus. Journal of Sound and Vibration. 2022; 527: 116818. doi: 10.1016/j.jsv.2022.116818
20. SheikhMozafari MJ. Enhancing Sound Absorption in Micro-Perforated Panel and Porous Material Composite in Low Frequencies: A Numerical Study Using FEM. Sound & Vibration. 2024; 58(1): 81-100. doi: 10.32604/sv.2024.048897
21. Sekar V, Yong Eh Noum S, Putra A, et al. Acoustic Properties of Micro-Perforated Panels Made from Oil Palm Empty Fruit Bunch Fiber Reinforced Polylactic Acid. Sound&Vibration. 2021; 55(4): 343-352. doi: 10.32604/sv.2021.014916
22. Ghanadi F, Arjomandi M, Cazzolato B, et al. Interaction of a flow-excited Helmholtz resonator with a grazing turbulent boundary layer. Experimental Thermal and Fluid Science. 2014; 58: 80-92. doi: 10.1016/j.expthermflusci.2014.06.016
23. Tam C, Kurbatskii K, Ahuja K, et al. R. A numerical and experimental investigation of the dissipation mechanisms of resonant acoustic liners. In: Proceedings of 7th AIAA/CEAS Aeroacoustics Conference and Exhibit; 28–30 May 2001; Maastricht,Netherlands.
24. Cummings A. Acoustic nonlinearities and power losses at orifices. AIAA Journal. 1984; 22(6): 786-792. doi: 10.2514/3.8680
25. Ji C, Zhao D. Two-dimensional lattice Boltzmann investigation of sound absorption of perforated orifices with different geometric shapes. Aerospace Science and Technology. 2014; 39: 40-47. doi: 10.1016/j.ast.2014.08.010
26. Zhu J, Qu Y, Gao H, et al. Nonlinear sound absorption of Helmholtz resonators with serrated necks under high-amplitude sound wave excitation. Journal of Sound and Vibration. 2022; 537: 117197. doi: 10.1016/j.jsv.2022.117197
27. Singh DK, Rienstra SW. Nonlinear asymptotic impedance model for a Helmholtz resonator liner. Journal of Sound and Vibration. 2014; 333(15): 3536-3549. doi: 10.1016/j.jsv.2014.03.013
28. Zhang Z, Zhao D, Han N, et al. Control of combustion instability with a tunable Helmholtz resonator. Aerospace Science and Technology. 2015; 41: 55-62. doi: 10.1016/j.ast.2014.12.011
29. Li L, Guo Z, Zhang C, Sun X. A Passive Method to Control Combustion Instabilities with Perforated Liner. Chinese journal of aeronautics. 2010; 23: 623-630. doi: 10.1016/S1000-9361(09)60263-6
30. Meng S, Zhang M, Gao Y. Influence of the Acoustic Liner in Large Eddy Simulation of Longitudinal Thermoacoustic Instability in a Model Annular Combustor. Journal of Thermal Science. 2024; 33(2): 710-724. doi: 10.1007/s11630-024-1928-x
31. Gullaud E, Nicoud F. Effect of Perforated Plates on the Acoustics of Annular Combustors. AIAA Journal. 2012; 50(12): 2629-2642. doi: 10.2514/1.j050716
32. Howe MS. On the theory of unsteady high Reynolds number flow through a circular aperture. The Royal Society of London a Mathematical and Physical Sciences. 1979; 366(1725): 205-223. doi: 10.1098/rspa.1979.0048
33. Meng S, Zhou H, Cen K. Application of the Perforated Plate in Passive Control of the Nonpremixed Swirl Combustion Instability Under Acoustic Excitation. Journal of Engineering for Gas Turbines and Power. 2019; 141(9). doi: 10.1115/1.4043848
34. Deshmukh NN, Kudachi B, Joy S, et al. Suppression of Thermo-Acoustic Instabilities using Helhmoltz Resonator. In: Proceedings of 2019 International Conference on Nascent Technologies in Engineering (ICNTE); 4-5 January 2019; Navi Mumbai, India.
35. Zalluhoglu U, Olgac N. A study of Helmholtz resonators to stabilize thermoacoustically driven pressure oscillations. The Journal of the Acoustical Society of America. 2016; 139(4): 1962-1973. doi: 10.1121/1.4946042
36. Betz M, Zahn M, Hirsch C, et al. Impact of Damper Placement on the Stability Margin of an Annular Combustor Test Rig. In: Proceedings of Volume 4A: Combustion, Fuels, and Emissions; 17-21 June 2019; Arizona, USA.
37. Aguilar JG, Dawson JR, Schuller T, et al. Locking of azimuthal modes by breaking the symmetry in annular combustors. Combustion and Flame. 2021; 234: 111639. doi: 10.1016/j.combustflame.2021.111639
38. Doria A. A Simple Method for The Analysis of Deep Cavity and Long Neck Acoustic Resonators. Journal of Sound and Vibration. 2000; 232(4): 823-833. doi: 10.1006/jsvi.1999.2763
39. Mohring J. Helmholtz resonators with large aperture. Acta Acustica united with Acustica. 1999; 85(6): 751-763.
40. Crandall LB. Theory of Vibrating Systems and Sound. Nature. 1927; 120(3024): 544-544. doi: 10.1038/120544b0